First-principle study origin of ferromagnetism in non-magnetic perovskite $BaSnO_3$ doped with 2p-X (X=C, N)

A. Guendouz*, K. Driss-Khodja, and B. Amrani

Laboratory of Theory and Simulation of Materials, Faculty of Exact and Applied Sciences, University of Oran 1 Ahmed Ben Bella, Oran, Algeria.

**e-mail: atikag512@yahoo.fr*

Received 7 November 2022; accepted 20 February 2024

In this study, our goal is to analyze the origin of magnetization in non magnetic cubic structure perovskite $BaSnO_3$ doped with 2p-X (X=C, N) using the full potential linearized augmented plane wave (FP-LAPW) method based on density functional theory (DFT). For the exchange and correlation potential we have applied two approaches: generalized gradient (GGA) and GGA plus-modified Becke and Johnson potential (mBJ-GGA). The results show that $BaSnO_3$ doped with C then with N and finally with C plus N exhibit half-metallic ferromagnetism behavior with the integer magnetic moment of 1, 2 and 3 μ_B per cell respectively. The origin of the ferromagnetism that occurs within these compounds is mainly caused by the p-p hybridization between 2p-impurities and its neighboring oxygen atoms. These results allowed to conclude that doped perovskite could provide a new type of materials, called half-metallic for future spintronics devices.

Keywords: $BaSnO_3$; first principles calculations; half-metallic; magnetic properties.

DOI: https://doi.org/10.31349/RevMexFis.70.061602

1. Introduction

Perovskite oxides of the general formula ABX_3 [1] have been the subject of much research in recent decades due to their potential applications in spintronics devices [2, 3]. Among these, $BaSnO_3$ is an important candidate because of their interesting proprieties such as wide band gap semiconductor ($E_g = 3.1-3.4$ eV) [4–6], high electron mobility at the room temperature is reported to be up to 320 $cm^2V^{-1}s^{-1}$ in bulk single crystal [7, 8] and up to 150 $cm^2V^{-1}s^{-1}$ in epitaxial thin films of La-doped $BaSnO_3$ [9], It is stable at high temperatures up to 1273 K [10, 11]. A high Seebeck coefficient of 58.9 μV/K was achieved for the Sb-substituted $BaSnO_3$ at 820 K [12].

Bouhemadou and Haddadi [13] studied the structural, elastic, electronic and thermal properties of $BaSnO_3$ using the first principles calculations. The electronic, structural and optical properties of perovskite $BaSnO_3$ have been studied using first principle calculations by Soleimanpour and Kanjouri [14]. S.Chahib *et al*. [15] studied the structural, electronic and optical properties of cobalt-doped $BaSnO_3$ by first principles calculations. Nandarapu Purushotham reddy and *et al.* [16] prepared and characterized Sb-doped $BaSnO_3$ for dye-sensitized solar cell. Yasukawa *et al.* [17] analyzed the thermoelectric properties of La-doped $BaSnO_3$ and they found the value of ZT equal to 0.11 at 1073 K. However, a deep study of the magneto-electronic properties of 2p-X(X= C, N) impurities in $BaSnO_3$ have not been done.

In this study, we are focusing on the possibility of the magnetization for non magnetic perovskite doped with impurities 2p-X (X= C, N).Our calculations are studied using the full-potential linearized augmented plane wave (FP-LAPW) method within the framework of density functional theory (DFT). The results reveal that our systems doping by C, N and C with N (Co-doped) present half-metallic behaviors with the integer magnetic moments about to 2.00 , 1.00 and 3.00 μ_B respectively.

Our paper is organized as follows: the computational details used in our calculations are presented in Sec. 2. Results and discussion are presented in Sec. 3. Finally a brief conclusion is given in Sec. 4.

2. Computational details

The perovskite $BaSnO_3$ crystallizes in a cubic structure (space group $Pm\bar{3}m$) where Ba , Sn and O atoms are located at Ba: 1b (1/2, 1/2, 1/2), Sn: 1a (0, 0, 0) and O: 3d (0, 0, 1/2) respectively. In order to simulate $BaSnO_{2.875}X_{0.125}$ compounds, we have composed a super-cell of 40 atoms then we replaced the O atom by 2p-X impurities (X= C, N) which are positioned in the middle of the super cell. Using first principle methods which are based on density functional theory (DFT), we have studied the ground state properties of doped and undoped $BaSnO_3$ compounds by applying the method of linearized augmented plane waves at total potential (FP-LAPW) which is implemented in the Wien2k code [17]. As exchange- correlation potential we have used the generalized gradient (GGA) [18] and the modified Becke-Johnson potential (mBJ-GGA) [19]. The values of the muffin-tin (MT) radii used for our calculations are 2.5, 2.3 and 1.6 u.a for Ba, Sn, O respectively. The parameter $R_{MT} \times K_{\max} = 8$ where R_{MT} is the average radius of the MT spheres and $K_{\max}$ is the magnitude of the largest k vector. Our self consistent calculations are repeated until the convergence energy is less than or equal to the value of 10^{-5} Ry as well as the limit of the convergence of charge is fixed at 10^{-4} e.

TABLE I. Tolerance factor t, lattice constant a, bulk modulus B and its pressure derivative B', enthalpy of the formation energy $\Delta H^0 f$ and bonds length of the cubic perovskite $BaSnO_3$ compared with the experimental data and other theoretical works.

$BaSnO_3$			
	Our work	Exp	Theo
t	1.021		
a(Å)	4.1917	4.116 [22]	4.1916 [13]
			4.156, 4.186 [24]
B(GPa)	144.6	145.8 [22]	144 [13]
B'	3.75		3.78 [13]
$\Delta H^0 f$ (KJ/ mol)	-16.6		
Sn-O(Å)	2.088	2.058 [25]	22.028 [26], 2.071 [27]
Ba-O(Å)	2.954	2.910 [25]	2.868 [26], 2.929 [27]
Ba-Sn(Å)	3.618	3.564 [25]	3.512 [26],3.587 [27]

3. Results and discussion

3.1. Structural properties

In order to determine the stability of $BaSnO_3$ perovskite in cubic phase, we have firstly calculated the Goldschmidt tolerance (t) factor [20] using the formula:

$$t = \frac{(r_{Ba} + r_O)}{\sqrt{2}\,(r_{Sn} + r_O)}. \qquad (1)$$

The ionic radii are $r_{Ba^{2+}} = 1.61$ Å, $r_{Sn^{4+}} = 0.69$ Å and $r_{O^{2-}} = 1.4$ Å [21]. The divergence of the tolerance factor t with respect to the unit decreases the prospect of forming the cubic phase as the stable structure. However; it increases the prospect of forming less symmetrical states. The value of the tolerance factor t obtained for $BaSnO_3$ is equal to 1.021 (Table I). Therefore, the structure of our material is cubic since the value of t is between 0.99 and 1.06. On the other hand, the thermodynamic stability of perovskite $BaSnO_3$ was confirmed by calculating the enthalpy of the formation energy $\Delta H^0 f$ by using the following equation:

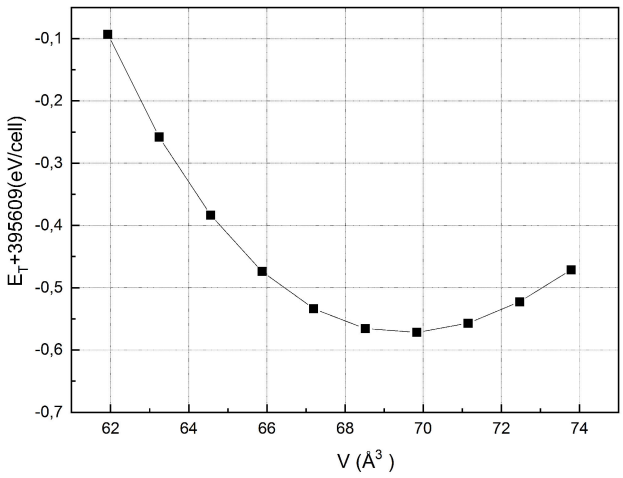

FIGURE 1. The total energy versus volume of $BaSnO_3$.

$$\Delta H^0 f = E_T^{BaSnO_3} - \left(E_T^{Ba} + E_T^{Sn} + \frac{3}{2}E_T^{O_2}\right), \qquad (2)$$

$E_T^{\mathrm{BaSnO_3}}$, E_T^{Ba}, E_T^{Sn} and $E_T^{\mathrm{O_2}}$ represents the minimum total energy of the $BaSnO_3$, Ba, Sn and O_2 respectively. From the results reported in Table I, the energy of formation of $BaSnO_3$ is negative and this confirms its thermodynamic stability, taking into consideration that this compound has already been synthesized experimentally [22].

In order to find the ground states properties of $BaSnO_3$ such as the lattice parameter a, bulk modulus B and its first pressure derivative B', we optimize the total energy for different volume which will then be adjusted to the Murnaghan equation of state [23] as shown in Fig. 1. The lattice parameter; bulk modulus and its first pressure derivative are given in Table I. It is clear that the lattice constant is underestimated from the experimental results of 1% . The small difference between the experimental and theoretical lattice constant shows the reliability of our theoretical work. The bulk modulus B obtained is in good agreement with the experimental work [22] and theoretical investigations [13, 24].

Turning now, to the average bond distances in $BaSnO_3$ perovskite, as mentioned in Table I. The results obtained are in good agreement with the experimental and theoretical values cited in the references [25, 26].

3.2. Mechanical stability and isotropic character

The elastic constants play an important role in determining the mechanical properties and offer information about the stability and the stiffness of the materials. By using the volume conserving tetrahedral and rhombohedral distortions on the cubic structure [28,29], we can calculate the elastic constants, into three independent ones named C_{11}, C_{12} and C_{44}. The traditional mechanical stability in this cubic structure leads to the following restrictions on the elastic constants [30]:

TABLE II. Elastic constants C_{ij}, the shear modulus G, young modulus E, Poisson ratio, Zener coefficient A and Pugh ratio B/G of $BaSnO_3$. The units for C_{ij}, G, and E are gigapascals.

	$BaSnO_3$		
	Our work	Exp	Theo
C_{11}	261.4	-	251.0 [27],358.5 [13], 285.2 [13]
C_{12}	85.75	-	82.3 [27], 93.5 [13], 68.5 [13]
C_{44}	87.38	-	98.1 [27], 110.3 [13], 84.3 [13]
G	87.55	99.9 [22]	118.7 [13] ,93.2 [13], 84 [24]
E	218.47	244 [22]	292.4 [13],229.1 [13], 207 [24]
v	0.24	-	0.232 [13], 0.229 [13], 0.23 [24]
A	0.99	-	1.16 [27], 0.83 [13], 0.78 [13]
B/G	1.65	-	1.53 [13],1.51 [13].

$$C_{11} - C_{12} > 0, \quad C_{44} > 0,$$
$$C_{11} + 2C_{12} > 0, \quad C_{12} < B < C_{11}. \tag{3}$$

According to the results of Table II, the compound $BaSnO_3$ is mechanically stable because the satisfaction of these stability conditions. Moreover, our elastic constants achieve in agreement with the other results available in the literature [13, 27]. On the other hand, the bulk modulus calculated from theoretical values of elastic constant: $B = 1/3(C_{11} + 2C_{44})$ for this compound corresponds to that obtained in the fit Murnaghan equation [23].

Moving now to the mechanical properties, the shear modulus G which describes the response to shear stress, the young modulus E represents the ability of a material to deform elastically, Poisson's ratio v which can give an idea about the nature of the deformation have been calculated and presented in Table II. The relationship between these parameters and elastic constants are displayed as follows [30–33]:

$$E = \frac{9BG}{3B+G}, \tag{4}$$

$$G = \frac{G_V + G_R}{2} \begin{cases} G_R = \frac{5C_{44}(C_{11}-C_{12})}{[4C_{44}+3(C_{11}-C_{12})]} \\ G_V = \frac{[C_{11}-C_{12}+3C_{44}]}{5} \end{cases} \tag{5}$$

$$v = \frac{3B-2G}{2(3B+G)}. \tag{6}$$

The Brittle and ductile nature of a material, Pugh [34] proposed an empirical relationship of B/G where the shear modulus G represents the resistance to plastic deformation while B shows the resistance to fracture. According to him, if the B/G ratio is greater than 1.75 the material is considered to be ductile, otherwise is brittle. So, we deduce from the Table II that this compound is classified as a brittle material.

Frantsevich [35] separated the ductility and the brittleness of materials in terms of Poisson's ratio and according to their rule, the critical value is equal to 0.26 as barrier term, if the Poisson's ratio is lower than this value, the compound is brittle otherwise it is ductile. From Table II, the value of the Poisson's ratio is observed to be 0.24 indicating that the fragility of this compound which supports the above conclusion.

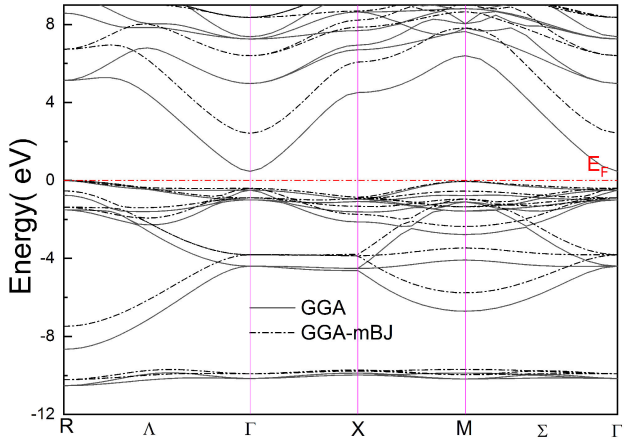

FIGURE 2. Band structures of $BaSnO_3$ with GGA and mBJ-GGA. The Fermi level is located at 0 eV.

Another important parameter is a shear anisotropic factor A (also named Zener coefficient) that gives a measure of the anisotropy of the elastic wave velocity in the crystal and is given by the following expression:

$$A = \frac{2C_{44}}{(C_{11} - C_{12})}. \tag{7}$$

For an isotropic crystal A is equal to 1 while the deviation of A from unity indicates the anisotropic nature. From Table II, it can be observed that the Zener anisotropy factor of $BaSnO_3$ is equal to 0.99, a value close to unity which allows us to conclude that our compound is elastically isotropic.

3.3. Band structures and density of states

The electronic properties of a compound can be studied from the band structure and density of states. The band structures

TABLE III. Calculated exchange constants with GGA and mBJ-GGA for $BaSnO_{2.875}C_{0.125}$, $BaSnO_{2.875}N_{0.125}$ and $BaSnO_{2.75}C_{0.125}N_{0.125}$.

	GGA		mBJ-GGA	
	$N_{0\alpha}$	$N_{0\beta}$	$N_{0\alpha}$	$N_{0\beta}$
$BaSnO_{2.875}C_{0.125}$	1.39	-1.15	1.47	-1.65
$BaSnO_{2.875}N_{0.125}$	0.98	-1.89	1.08	-2.07
$BaSnO_{2.75}C_{0.125}$ $N_{0.125}$	0.61	-0.45	0.97	-0.68

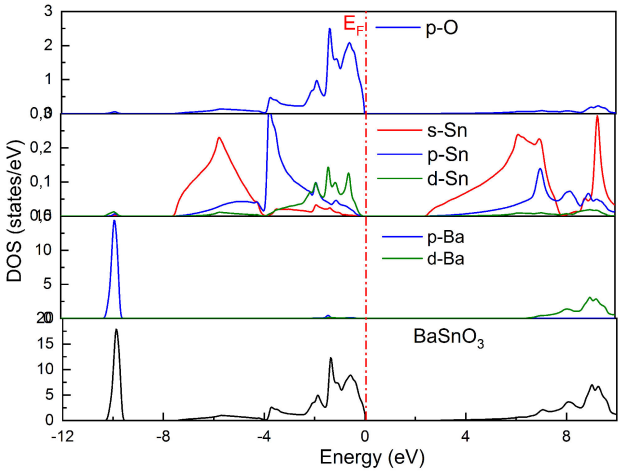

FIGURE 3. The total density of states and partial of $BaSnO_3$.

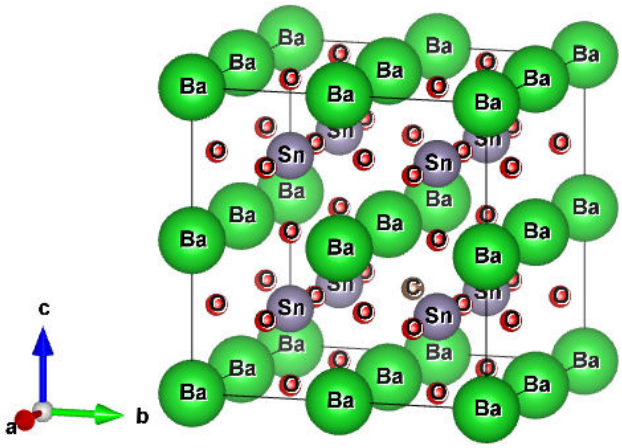

FIGURE 4. Cubic structure of $BaSnO_{2.875}C_{0.125}$.

for $BaSnO_3$ along the high symmetry direction in the first Brillouin zone are calculated by using GGA and mBJ-GGA approaches (Fig. 2). We can observe that the calculations of the band structures by both approximations are identical but the calculations obtained by mBJ gives a clear improvement in the value of the gap energy. The top of the valence band is positioned at R point and the bottom of the conduction band is located at (Γ) point. As a result this compound has an indirect band gap $(R-\Gamma)$ which is consistent with refs [22,27,36]. The value of the indirect gap energy $(R-\Gamma)$ calculated by the GGA approximation is equal to 0.65 eV and the direct gap $(\Gamma-\Gamma)$ is equal to 1.1 eV. The results obtained are in good agreement with other calculations [22,27,36] but they have lowered the experimental value [4, 6]. Based on our results and literature, the GGA approximation strongly underestimates the value of the band gap energy. To improve our results, we used mBJ approach which is a modified version of the exchange potential proposed by Becke and Johnson in order to give precise gaps very close to the experimental values [19]. By applying the mBJ approximation, we got the value of the indirect gap energy which is equal to 2.61 eV and the direct gap is 2.9 eV in which this last is close to the experimental value [4, 6].

To better understand the band structure of the studied, it is important to calculate density of the states. The total and partial densities of states are shown in Fig. 3. The energy zone located in the interval [-11.4; -9] eV is mainly due to the 2p-Ba and 4d-Sn orbitals. Then, the energy range -4 eV at the Fermi level is dominated by the 2p-O and 5p-Sn states. Finally, the conduction band is mainly due to the 5s-Sn and 5d-Ba states.

3.4. Electronic and magnetic properties of $BaSnO_3$ doped by C and N

In this part, we'll study the electronic and magnetic properties of the $BaSnO_3$ compound doped by non-magnetic 2p-impurities such as C, N and analysis the influence of these substitution impurities in our system. For this purpose, we create a super-cell containing 40 atoms in which the impurity 2p-X (X= C, N) replaces one oxygen atom centered in $BaSnO_3$ perovskite to obtain the system $BaSnO_{2.875}X_{0.125}$ (Fig. 4).

In order to confirm the stability of our compound in magnetic and non-magnetic states, we calculated the energy difference ΔE between spin-polarized and non-spin-polarized states. This difference is given by the following relation: $\Delta E = E_M - E_{NM}$ where E_M and E_{NM} are the total energies of the magnetic and non-magnetic states of our systems respectively. The different energy values ΔE for $BaSnO_3$ doped with C, N and C plus N are: -76.8, -530.4 and -892.8 meV respectively, which indicates that the magnetic states are more stable compared to non-magnetic states for our compound.

For deeper analysis the doping effects of 2p-impurities and the origins of the magnetic behaviors, we calculated the total and partial densities of states for the doped perovskite

TABLE IV. Calculated local, total magnetic moments (in Bohr magnetons μ_B) and polarization $P(\%)$ with GGA and mBJ-GGA for $BaSnO_{2.875}C_{0.125}$, $BaSnO_{2.875}N_{0.125}$ and $BaSnO_{2.75}C_{0.125}N_{0.125}$.

Compounds	Approach	M_{Ba}	M_{Sn}	M_O	M_X	M_{Tot}	P
$BaSnO_{2.875}C_{0.125}$	GGA	0.019	0.002	0.007	0.867	2.001	100
	mBJ-GGA	0.000	0.0002	0.0002	0.976	2.000	100
$BaSnO_{2.875}N_{0.125}$	GGA	0.009	0.003	0.006	0.537	1.000	100
	mBJ-GGA	0.0001	0.002	0.0004	0.651	1.000	100
$BaSnO_{2.75}C_{0.125}N_{0.125}$	GGA	0.005	0.001	0.005	0.848	3.001	100
					0.586		
	mBJ-GGA	0.0001	0.0006	0.0004	0.968	3.000	100
					0.671		

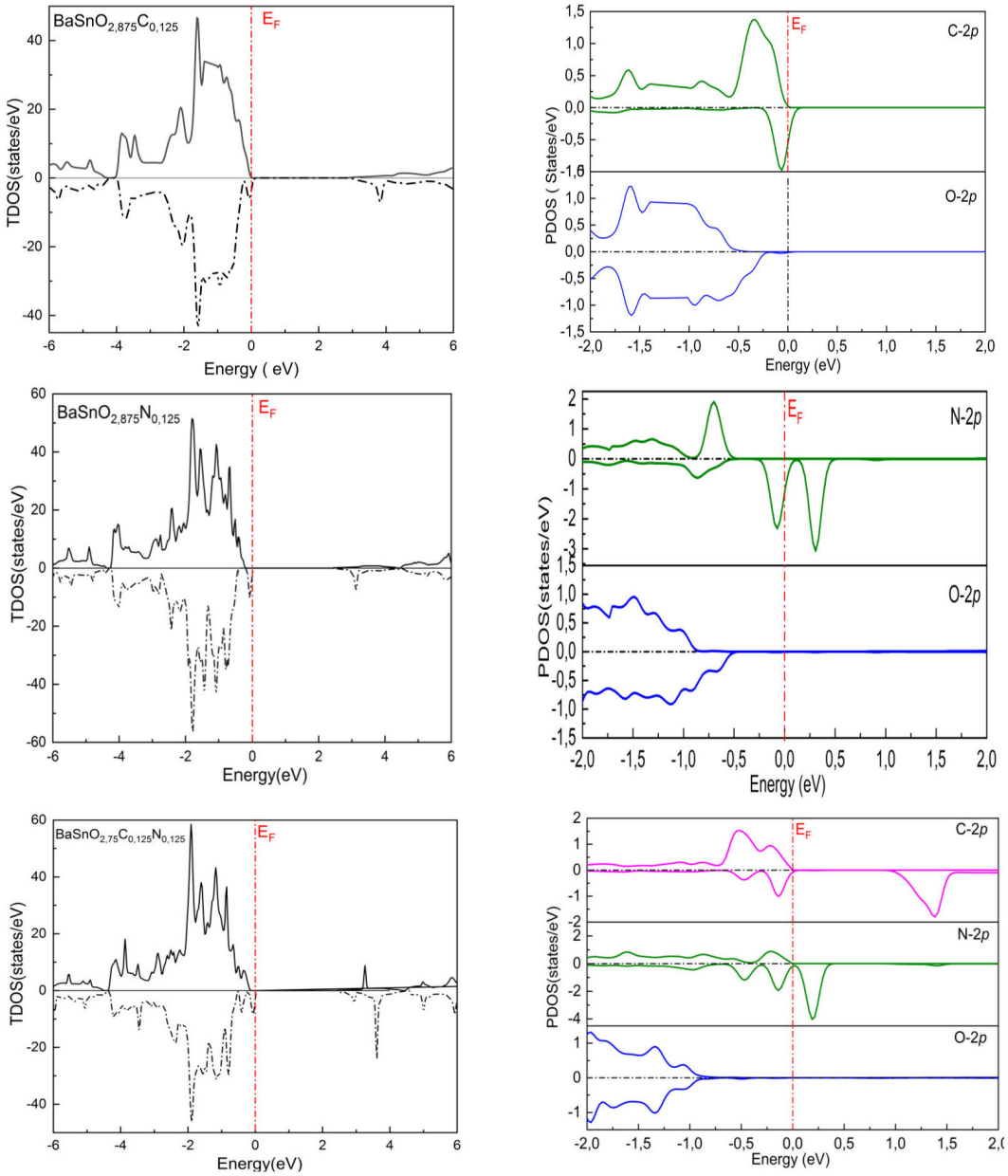

FIGURE 5. The total density of states and partial (spin up and spin down) of $BaSnO_{2.875}C_{0.125}$, $BaSnO_{2.875}N_{0.125}$ and $BaSnO_{2.75}C_{0.125}N_{0.125}$. The Fermi level is located at 0 eV.

using GGA and mBJ-GGA approximations. The figures of both functional GGA and mBJ-GGA are equivalent in shape. Therefore, only the results obtained through mBJ-GGA functional are presented in Fig. 5. That means, the cited compounds present half metallic behaviors when C and N atoms are included. On the other hand, these inclusions give an important magnetic moment for our systems where its origin is due to the hybridization between the 2p-impurities and its surrounding 2p-O.

3.5. Exchange coupling and magnetic properties

The ferromagnetic band structures can also be used to estimate two important parameters, the exchange constants $N_0\alpha$ (conduction band) and the exchange constant $N_0\beta$ (valance band). These exchange constants can be defined as [37, 38]:

$$N_0\alpha = \frac{\Delta E_c}{x\langle s\rangle}, \quad N_0\beta = \frac{\Delta E_v}{x\langle s\rangle}, \tag{8}$$

where ΔE_c, ΔE_v are the band-edge spin splitting of the conduction bands and valence bands respectively, x is the concentration of dopant and $\langle s\rangle$ denotes the average magnetization of the dopant atoms.

Our calculated values of $N_0\alpha$ and $N_0\beta$ are reported in Table III, they show that the exchange constants confirm the magnetic character of these compounds. Notice that, the exchange constants of the valence band and the conduction band obtained are in an opposite sign (Table III). That means that the valence band and the conduction band have an opposite behavior during the fission exchange process.

The calculations of the total magnetic moments for our systems give integer numbers which are in conformity with the half-metallic behavior of these compounds (Table IV). These total magnetic moments which come from the 2p-X (C, N) ions and originate from Hund's rule coupling are found to be equal to the number of doped holes and distributed mainly on the p-orbital near the neighboring dopant [39].Thus, it gives rise to a moment magnetic total equal to 2, 1 and 3 μ_B per unit cell for C, N and C plus N doped $BaSnO_3$ respectively. On the other hand, the values of the spin polarization are important ($P = 100\%$) which confirms the half-metallic character of our compound. It is important to stress that, to our knowledge, the scientific community has no experimental or theoretical value of magnetic moments for our compounds so we consider these results to be an early prediction.

4. Conclusion

To summarize, we have studied the magneto-electronic properties of 2p-X (C, N) impurities in perovskite $BaSnO_3$ by first principles calculations. According to Hund's rule, the calculations disclose that half-metallic ferromagnetism can lead to $BaSnO_3$ doped with 2p-X impurties. The total magnetic moments of $BaSnO_3$ doped with C, N and C plus N are 2.00, 1.00 and 3.00 μ_B per cell respectively and they are caused mostly by impurity atoms. The origin of the ferromagnetism that occurs within these compounds is mainly caused by the p-p hybridization between the X-impurities and the surrounding oxygen atoms. Our results show that these doped perovskites can reveal to a new type of materials, called half-metallic ferromagnets which are favorable materials for future spintronics devices.

Acknowledgement

The authors gratefully acknowledge support from the staff at the Intensive Computing Unit of Oran 1 University.

Declarations Conflict of interest

The authors declare no competing financial interest.

Data availability statement

The data that support the findings of this study are available from the corresponding author, upon reasonable request.

1. R.H.J. Mitchell, Perovskites: modern and ancient, (2002). https://doi.org/10.1107/S0108768102020220.

2. C.N.R. Rao, B. Raveau, Colossal magnetoresistance, charge ordering and related properties of manganese oxides, World Scientific 1998. https://doi.org/10.1142/3605.

3. Y.J.P.A. Tokura, Colossal Magnetoresistive Oxides, Gordon and Breach Science, (2000). https://doi.org/10.1201/9781482287493.

4. G. Larramona, C. Gutiérrez, I. Pereira, M.R. Nunes, F.M.A. da Costa, Characterization of the mixed perovskite $BaSn_1$-SbO_3 by electrolyte electroreflectance, diffuse reflectance, and X-ray photoelectron spectroscopy, Journal of the Chemical Society, *Faraday Transactions 1: Physical Chemistry in Condensed Phases* **85** (1989) 907, https://doi.org/10.1039/F19898500907.

5. H. Mizoguchi, H.W. Eng, P.M. Woodward, Probing the Electronic Structures of Ternary Perovskite and Pyrochlore Oxides Containing Sn^{4+} or Sb^{5+}, *Inorganic Chemistry* **43** (2004) 1667, https://doi.org/10.1021/ic034551c.

6. H. Mizoguchi, P.M. Woodward, C.-H. Park, D.A. Keszler, Strong Near-Infrared Luminescence in $BaSnO_3$, *Journal of the American Chemical Society* **126** (2004) 9796, https://doi.org/10.1021/ja048866i.

7. X. Luo, Y.S. Oh, A. Sirenko, P. Gao, T.A. Tyson, K. Char, S.-W. Cheong, High carrier mobility in transparent $Ba_{1-x}La_{1-x}SnO_3$ crystals with a wide band gap, *Ap-*

plied Physics Letters **100** (2012), https://doi.org/10.1063/1.4709415.

8. H.J. Kim, U. Kim, Kim, T.H. Kim, H.S. Mun, B.-G. Jeon, K.T. Hong, W.-J. Lee, C. Ju, K.H. Kim, K. Char, High Mobility in a Stable Transparent Perovskite Oxide, *Applied Physics Express* **5** (2012) 061102, https://doi.org/10.1143/APEX.5.061102.
9. S. James Allen, S. Raghavan, T. Schumann, K.-M. Law, S. Stemmer, Conduction band edge effective mass of La-doped $BaSnO_3$, *Applied Physics Letters* **108** (2016). DOI: 10.1063/1.4954671.
10. M.G. Smith, J.B. Goodenough, A. Manthiram, R.D. Taylor, W. Peng, and C.W. Kimball, Tin and antimony valence states in $BaSn_{0.85}Sb_{0.1503}$, *Journal of Solid State Chemistry* **98** (1992) 181, https://doi.org/10.1016/0022-4596(92)90084-9.
11. B. Ostrick, M. Fleischer, U. Lampe, H. Meixner, Preparation of stoichiometric barium stannate thin films: Hall measurements and gas sensitivities, *Sensors and Actuators B: Chemical* **44** (1997) 601, https://doi.org/10.1016/S0925-4005(97)00141-X.
12. P. Rajasekaran, Y. Kumaki, M. Arivanandhan, M.M.S. Ibrahim Khaleeullah, R. Jayavel, H. Nakatsugawa, Y. Hayakawa, M. Shimomura, Effect of Sb substitution on structural, morphological and electrical properties of $BaSnO_3$ for thermoelectric application, *Physica B: Condensed Matter* **597** (2020) 412387, https://doi.org/10.1016/j.physb.2020.412387.
13. A. Bouhemadou, K. Haddadi, Structural, elastic, electronic and thermal properties of the cubic perovskite-type $BaSnO_3$, *Solid State Sciences* **12** (2010) 630, https://doi.org/10.1016/j.solidstatesciences.2010.01.020.
14. S. Soleimanpour, F. Kanjouri, First principle study of electronic and optical properties of the cubic perovskite $BaSnO_3$, *Physica B: Condensed Matter* **432** (2014) 16, DOI:https://doi.org/10.1016/j.physb.2013.09.004.
15. S. Chahib, D. Fasquelle, G. Leroy, Density functional theory study of structural, electronic and optical properties of cobalt-doped $BaSnO_3$, *Materials Science in Semiconductor Processing* **137** (2022) 106220.DOI:https://doi.org/10.1016/j.mssp.2021.106220.
16. P. Rajasekaran *et al*., The effect of rare earth ions on structural, morphological and thermoelectric properties of nanostructured tin oxide based perovskite materials, *Materials Research Express* **4** (2017) 115024, https://doi.org/10.1088/2053-1591/aa97a1.
17. P. Blaha, K. Schwarz, G.K.H. Madsen, D. Kuasnicke, J. Luitz, Introduction to WIEN2K, An Augmented plane wane plus local orbitals program for calculating crystal properties (Vienna university of technology, Vienna, Austria, 2001) (2001).
18. J.P. Perdew, K. Burke, M. Ernzerhof, Generalized Gradient Approximation Made Simple, *Physical Review Letters* **77** (1996) 3865, https://doi.org/10.1103/PhysRevLett.77.3865.
19. F. Tran, P. Blaha, K. Schwarz, P. Novák, Hybrid exchange-correlation energy functionals for strongly correlated electrons: Applications to transition-metal monoxides, *Physical Review B* **74** (2006) 155108, https://doi.org/10.1103/PhysRevB.74.155108.
20. V. Goldschmidt, Die Gesetze der Krystallochemie. *Naturwissensenschaffen,* **14** (1926) 477, DOI: https://doi.org/10.1007/BF01507527.
21. R.D. Shannon, C.T. Prewitt, Effective ionic radii in oxides and fluorides, Acta *Crystallographica Section B* **25** (1969) 925, https://doi.org/10.1107/S0567740869003220.
22. T. Maekawa, K. Kurosaki, S. Yamanaka, Thermal and mechanical properties of polycrystalline $BaSnO_3$, *Journal of Alloys and Compounds*, **416** (2006) 214, https://doi.org/10.1016/j.jallcom.2005.08.032.
23. F.D. Murnaghan, *The Compressibility of Media under Extreme Pressures*, **30** (1944) 244, https://doi.org/10.1073/pnas.30.9.244.
24. E. Bévillon, A. Chesnaud, Y. Wang, G. Dezanneau, G. Geneste, Theoretical and experimental study of the structural, dynamical and dielectric properties of perovskite $BaSnO_3$, *Journal of Physics: Condensed Matter* **20** (2008) 145217, https://doi.org/10.1088/0953-8984/20/14/145217.
25. H.M. Elizabeth, J.P. Attfield, A.T.R. Simon, Cation-size control of structural phase transitions in tin perovskites, *Journal of Physics: Condensed Matter* **15** (2003) 8315, https://doi.org/10.1088/0953-8984/15/49/010.
26. E. Moreira *et al*., Structural and electronic properties of $Sr_xBa_{1-x}SnO_3$ from first principles calculations, Journal of Solid State Chemistry **187** (2012) 186, https://doi.org/10.1016/j.jssc.2011.12.027.
27. J. Tang, J. Ye, W. Zhang, Structural, photocatalytic, and photophysical properties of perovskite $MSnO_3$ (M = Ca, Sr, and Ba) photocatalysts, *J. Materials Research* **22** (2007) 1859, https://doi.org/10.1557/jmr.2007.0259.
28. M.J. Mehl, J.E. Osburn, D.A. Papaconstantopoulos, B.M. Klein, Structural properties of ordered high-melting-temperature intermetallic alloys from first-principles total-energy calculations, *Physical Review B* **41** (1990) 10311, https://doi.org/10.1103/PhysRevB.41.10311.
29. M.J. Mehl, B.M. Klein, D.A. Papaconstantopoulos, Intermetallic compounds: principle and practice, *Principles* **1** (1995) 195.
30. M. Born, K. Huang, Dynamical Theory Of Crystal Lattices, Oxford University Press 1996.
31. R. Hill, The Elastic Behaviour of a Crystalline Aggregate, *Proceedings of the Physical Society. Section A* **65** (1952) 349. https://doi.org/10.1088/0370-1298/65/5/307.
32. W. Voigt, Lehrbuch der kristallphysik: Teubner-Leipzig [M], Macmillan New York, 1928.
33. A. Reuss, Berechnung der Fließgrenze von Mischkristallen auf Grund der *Plastizitätsbedingung fÃ¼r Einkristalle*, **9** (1929) 49, https://doi.org/10.1002/zamm.19290090104.
34. S.F. Pugh, XCII. Relations between the elastic moduli and the plastic properties of polycrystalline pure metals, *The London, Edinburgh, and Dublin Philosophical Magazine and Journal of Science* **45** (1954) 823-843. https://doi.org/10.1080/14786440808520496.

35. I.N. Frantsevich, F.F. Voronov, S.A. Bakuta, Elastic constants and elastic moduli of metals and nonmetals(In Russian), Kiev, *Izdatel'stvo Naukova Dumka*, **1982**, (1982) 288.

36. D.J. Singh, D.A. Papaconstantopoulos, J.P. Julien, F. Cyrot-Lackmann, Electronic structure of Ba(Sn,Sb)O_3: Absence of superconductivity, *Physical Review B* **44** (1991) 9519, https://doi.org/10.1103/PhysRevB.44.9519.

37. S. Sanvito, P. Ordejón, N.A. Hill, First-principles study of the origin and nature of ferromagnetism in $Ga_{1-x}Mn_xAs$, *Phys. Rev. B* **63** (2001) 165206, https://doi.org/10.1103/PhysRevB.63.165206.

38. H. Raebiger, A. Ayuela, R.M. Nieminen, Intrinsic hole localization mechanism in magnetic semiconductors, *Journal of Physics: Condensed Matter* **16** (2004) L457. https://doi.org/10.1088/0953-8984/16/41/L05.

39. T. Cao, Z. Li, S.G. Louie, Tunable Magnetism and Half-Metallicity in Hole-Doped Monolayer GaSe, *Physical Review Letters* **114** (2015) 236602. https://doi.org/10.1103/PhysRevLett.114.23660.